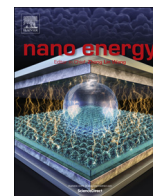




ELSEVIER

Contents lists available at ScienceDirect

## Nano Energy

journal homepage: [www.elsevier.com/locate/nanoen](http://www.elsevier.com/locate/nanoen)

# Triboelectric liquid volume sensor for self-powered lab-on-chip applications



Hao Wang<sup>a,b,c</sup>, Zhuolin Xiang<sup>a,b,c</sup>, Pastorin Giorgia<sup>d</sup>, Xiaojing Mu<sup>e,\*</sup>, Ya Yang<sup>f</sup>,  
Zhong Lin Wang<sup>g</sup>, Chengkuo Lee<sup>a,b,c,\*\*</sup>

<sup>a</sup> Department of Electrical and Computer Engineering, National University of Singapore, 4 Engineering Drive 3, 117576, Singapore

<sup>b</sup> Center for Sensors and MEMS, National University of Singapore, 4 Engineering Drive 3, 117576, Singapore

<sup>c</sup> NUS Suzhou Research Institute (NUSRI), Suzhou Industrial Park, Suzhou 215123, PR China

<sup>d</sup> Department of Pharmacy, National University of Singapore, 18 Science Drive 4, 117543, Singapore

<sup>e</sup> Key Laboratory of Optoelectronic Technology & Systems, Ministry of Education, Defense Key Disciplines Lab of Novel Micro-nano Devices and Systems Technology, International R&D center of Micro-nano Systems and New Materials Technology, Chongqing University, 400044, PR China

<sup>f</sup> Beijing Institute of Nanoenergy and Nanosystems, Chinese Academy of Sciences, Beijing 100083, PR China

<sup>g</sup> School of Materials Science and Engineering, Georgia Institute of Technology, Atlanta, Georgia 30332, USA

## ARTICLE INFO

### Article history:

Received 5 October 2015

Received in revised form

23 November 2015

Accepted 28 February 2016

Available online 16 March 2016

### Keywords:

Triboelectric energy harvester

Triboelectric liquid volume sensor

Drug delivery patch

## ABSTRACT

Technology for enabling drug delivery with precise control is strongly demanded by patients with diabetes or other chronic diseases. More intelligent functions such as drug loading and delivery in controllable manner without requiring electrical power will make low-cost drug delivery patches come true. One of the promising candidates is triboelectric technology which has been deployed as nanogenerators and self-powered glucose sensors recently. In this paper, the drug delivery is triggered by finger-pressing on a polymer based micropump. Considering that the finger-pressing should be an action of very low frequency, e.g., 1 to 2 Hz, triboelectric energy harvester (TEH) based on contact-separation mode between patterned biocompatible polymer layer and Aluminum (Al) film is integrated with microneedles on a flexible skin patch. Leveraging triboelectric materials and compatible fabrication technology, we successfully develop a self-powered flexible skin patch for transdermal insulin delivery with novel liquid volume sensor to monitor delivered drug volume and flexible energy harvester using the same triboelectric mechanism. With 3stacked polymer layers, the TEH of  $2 \times 2 \text{ cm}^2$  area generates 33  $\mu\text{W}$  by gentle finger tapping at 2 Hz. Such energy could be harvested even during drug delivery via finger pressing. In future we can further store harvested energy in a battery to provide required operation power for other active components or glucose sensors integrated in this skin patch. The developed flexible skin patch for transdermal drug delivery is further validated by in vivo experiments in rats.

© 2016 Elsevier Ltd. All rights reserved.

## 1. Introduction

Wearable medical devices based on lab-on-chip (LoC) technology have received major attention recently owing to their considerable practicability for health monitoring and disease treatment [1–3]. The interest, within the medical community, for wearable medical monitoring systems arises from the need of monitoring patients from a distance and over long periods of time. Such on-body monitoring devices can alert the patient of any imminent health hazard and hence facilitate rapid corrective clinical action outside of the hospital environment. Currently, several wearable

\*\* Corresponding author at: Department of Electrical & Computer Engineering, National University of Singapore, 4 Engineering Drive 3, 117576, Singapore.

\* Corresponding author.

E-mail addresses: [elelc@nus.edu.sg](mailto:elelc@nus.edu.sg) (X. Mu), [elelc@nus.edu.sg](mailto:elelc@nus.edu.sg) (C. Lee).

sensors for health monitoring have been explored, including devices that measure hydration [4], strain [5], glycaemia [6–8], metabolic acid [9] and cardiorespiratory signals [10]. While these medical devices monitor important health parameters, there is strong need for wearable systems designed for chronic diseases treatment such as hypertension, osteoporosis and diabetes. In such cases, the patients are preferably to have convenient means for self-administered transdermal drug delivery. Several kinds of skin patches have been developed and demonstrated to fulfill these requirements such as microneedle skin patch for insulin delivery [11,12] and pain patch to relief pain [13]. With the drug coated on the surface, these skin patches are suitable for self-administrated drug delivery. Meanwhile, the drug coating method can only provide limited drug volume and the dose to be delivered also cannot be controlled.

However, for the treatment of diseases such as type 2 diabetes and osteoporosis, multiple drug injections per day with dose

control of each injection will be necessary. The skin patches mentioned above cannot fully meet these requirements. Thus, large delivery volume and a precise control mechanism are desirable features for wearable skin patch drug delivery system but not developed yet. It means within the skin patch, a liquid volume sensor with proper mechanism should be integrated with the fluidic system for drug loading and delivery. Moreover, a standalone wearable drug delivery skin patch with capability of health monitoring, signal processing and interfacing with external cloud computing apparatus, an built-in energy source is inevitable to power components such as integrated circuits (ICs), microprocessor, liquid-crystal display (LCD) reading panel, drug delivery and control actuators, and diversified sensors, e.g., glucose sensor [14].

Here, we report a LoC drug delivery patch with manually-controlled drug delivery function and power source which is suitable for further integration with other active components for more applications. The key innovation of our design is that the liquid volume could be sensed by a triboelectric mechanism using the same materials for LoC. Thus the delivery volume can be well measured and controlled during the drug delivery process. A microneedle array was assembled onto the patch to confirm the drug control function by insulin delivery tests on rats. To make the patch able to maintain a tight and stable contact with the contoured and deformable skin surface, the whole device is made of PDMS, a known biocompatible soft and flexible material. By leveraging the similar triboelectric mechanism as the liquid sensor, we developed and optimized a stacked layer design triboelectric energy harvester (TEH) which is suitable to be attached onto the patch as an energy source. Such energy source can be used to support the operation of other components.

## 2. Experiment

### 2.1. Design structure and working principle of triboelectric liquid volume sensor

We propose a LoC drug delivery patch with manually-con-

trolled drug delivery and dose volume monitoring as shown in Fig. 1(A). The microfluidics control system has four parts: two check-valves in series, a pneumatic pump-chamber between these two check-valves, several drug reservoirs in series and microfluidic channels connecting all these components. By pressing the pump chamber, the liquid will be sucked into the channel from the inlet and delivered out from the outlet as shown in Fig. 1(A). The detailed structure and working principle are shown in Fig. S1.

A TEH, which is the main component of the liquid volume sensor, was integrated above the pump chamber. Although TEH based liquid flow sensor has been studied [15]. The proposed liquid volume sensor using the triboelectric sensing mechanism has not been demonstrated yet. Currently, the triboelectric sensing mechanism has been investigated in terms of chemical sensor [14,16–18], pressure sensor [19–21], motion sensor [22–28] and tactile sensor [29–31] because of its advantage of easy fabrication and self-powered feature. Here we assembled a triboelectric layer pair with the same area as the pump chamber, i.e., of  $1.2 \times 1.2 \text{ cm}^2$  for sensing liquid volume. The working principle and detailed structure of the fabricated delivery volume sensor is depicted in Fig. 1(B). The fabrication process of the TEH with one layer triboelectric pair is shown in Fig. S2.

Fig. 1(B) shows a detailed structure of the TEH assembled for liquid volume sensor. A dielectric PDMS layer with pyramid shape micro-patterns was used to enhance the surface area and output voltage. Underneath the PDMS layer, a Kapton tape was attached as an intermediary layer for metal deposition. To have a better adhesion between Cu and Kapton, a Cr layer was deposited before the deposition of Cu layer. In order to protect the metal layer, a parylene layer was coated by CVD onto the whole surface of the TEH, including the PDMS top surface. Then the TEH was assembled in a PDMS chamber with Al layer coated on the ceiling.

In the original position, the surface of the TEH and ceiling are not in contact (Fig. 1(a1) and (b1)). When the bottom layer of the pump chamber is pressed, the liquid or the air in the in the pump chamber will be compressed and the top layer of the pump chamber will also be deformed. This deformation will induce a contact between the top layer of the TEH and the ceiling of the

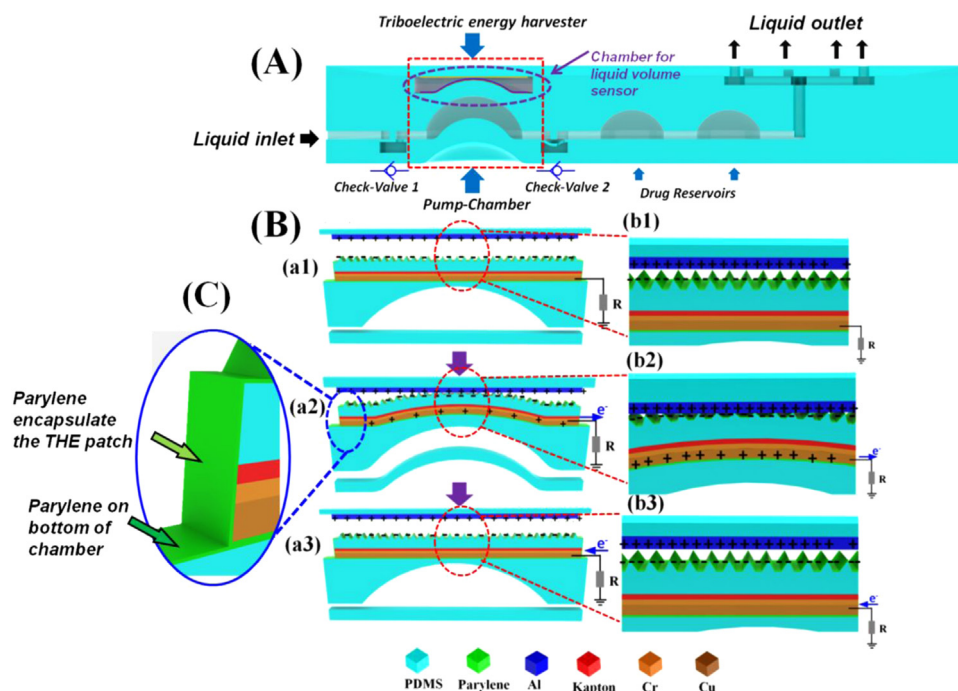


**Fig. 1.** (A) Cross-sectional view of the lab-on-chip drug delivery patch; (B) Working principle of the TEH for the delivery volume sensor; (b1) to (b3) shows the a magnification of layer structure and charge polarity in (a1) to (a3); (C) Detailed image shows the parylene layer to encapsulate the TEH patch and coated on the bottom of the chamber.

PDMS chamber, resulting in charge transport between them (Fig. 1 (a2) and (b2)). According to the triboelectric theory, electrons are transferred from the parylene to the Al during the electrification process, since parylene is triboelectrically negative and Al is triboelectrically positive. The change of the negative charges on the surface of the parylene can induce positive charges on the Cu electrode, driving free electrons to flow from the Cu layer to the ground. An output voltage or signal is generated. Once the pressing is released, the parylene and Al surfaces are separated (Fig. 1 (a3) and (b3)). The recovery of the surface negative charge on parylene surface will induce a backflow of electrons from ground to Cu electrode. An opposite signal will be generated. The output voltage is generated by the contact between parylene and Al and it is determined by the contact area. And this contact area is also determined by the deformation of the pump-chamber, which is related with the delivery volume. Thus, based on the output signal, the delivery volume can be measured.

To avoid the interference from the backside of the TEH, the bottom of the chamber is also coated with parylene as shown in Fig. 1(C). Thus, the backside of the TEH and the bottom surface of the chamber are of the same material. The contact of these two interfaces will not generate any output voltage.

To achieve the highest voltage, the surface materials of the triboelectric layer pair should be optimized. The gap between the top and bottom of the delivery volume sensor is critical to measurement accuracy of the liquid volume sensor. To ensure a good accuracy of this delivery volume sensor, this gap is also optimized.

### 3. Result and discussion

#### 3.1. Optimization and characterization of the surface materials of the triboelectric layer pair

To enhance the sensitivity of the delivery volume sensor, the output voltage of the TEH is expected to be as high as possible. Here we investigated the effect of surface pyramid micro-pattern, material of contact surface and the thickness of the PDMS dielectric layer. Three groups of samples with different PDMS thickness are prepared as shown in the Table 1.

In the test, the TEH patches were fixed onto a force gauge and applied onto the PDMS or Al contact surface with the same force, which is 10 N. To make the open circuit output voltage of TEH reaches the maximum value, the surface of TEH is fully contacted with PDMS or Al surface.

The experimental measurement data is shown in Fig. 2(a). According to the  $V-Q-x$  relationship for contact-mold TEHs [32], the output voltage is determined by the following equation:

$$V = E_{\text{dielectric}} \times d + E_{\text{air}} \times x \quad (1)$$

where  $E_{\text{dielectric}}$  is the electric field though the dielectric layer generated by the tribo-charges on the opposite sides of the TEH;  $d$  is the thickness of the dielectric layer;  $E_{\text{air}}$  is the electric field though the spacing between the top surface of TEH and contact surface, this electric field is generated by the tribo-charges on the TEH surface and contact surface;  $x$  is the spacing between the TEH surface and contact surface. The output voltage should increase with the increase of the dielectric layer thickness in the ideal fully contact-mold TEHs.

For group 1, there is no pyramid micro-pattern on the surface of TEH. The two contact surfaces are parylene and PDMS. The output voltage increases from 3.8 V to 9.5 V when the thickness of PDMS dielectric layer increases from 30  $\mu\text{m}$  to 215  $\mu\text{m}$ , which is consistent with the Eq. (1).

For group 2, there are pyramid micro-patterns on the surface of

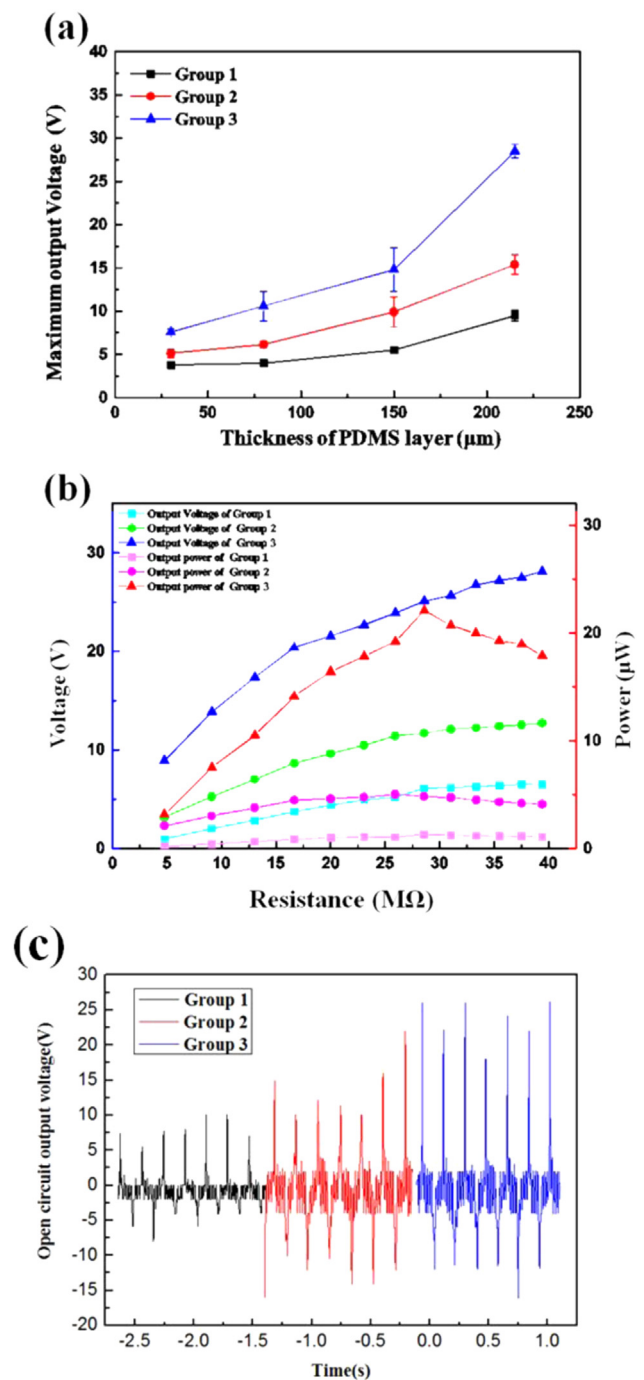


Fig. 2. (a) Optimization for PDMS thickness and material of contact surfaces; (b) Characterization of the output power; (c) Output voltage over time of the different triboelectric surface pairs when the thickness of the PDMS layer is 200  $\mu\text{m}$ .

TEH. The two contact surfaces are the same as group 1. Compared with the samples of group 1, the output voltages of the samples of group 2 have about 50% enhancement with the same PDMS thickness. The output voltage increases from 5.2 V to 14.6 V when the thickness of the PDMS dielectric layer increases from 30  $\mu\text{m}$  to 215  $\mu\text{m}$ . Thus the pyramid micro-pattern on the surface of TEH can enhance the output voltage by 50%.

The samples of group 3 are the same as group 2. To further increase the output voltage, we changed another contact surface from PDMS to Al. Since Al is more triboelectrically positive than PDMS, these contact surfaces of parylene and Al could generate higher output voltage. For the samples of 30  $\mu\text{m}$ , 80  $\mu\text{m}$  and

**Table 1**  
Details of groups of sample for optimization of PDMS thickness and contact surfaces.

Group no.	Surface micro-pattern	Contact surface	Thickness of dielectric layer
Group 1	Without pyramid micro-pattern	Parylene vs PDMS	30 $\mu\text{m}$
			80 $\mu\text{m}$
			150 $\mu\text{m}$
			215 $\mu\text{m}$
Group 2	With pyramid micro-pattern	Parylene vs PDMS	30 $\mu\text{m}$
			80 $\mu\text{m}$
			150 $\mu\text{m}$
			215 $\mu\text{m}$
Group 3	With pyramid micro-pattern	Parylene vs Al	30 $\mu\text{m}$
			80 $\mu\text{m}$
			150 $\mu\text{m}$
			215 $\mu\text{m}$

150  $\mu\text{m}$ , the output voltages are about 50% higher than their counterparts of group 2. For the sample of 215  $\mu\text{m}$  thickness, the output voltage has 100% enhancement than the sample with the same thickness of group 2. This maybe induced by the too thick layer of PDMS. During the test, not only the surface pyramid micro-patterns get deformation, but the PDMS layer itself also got serious deformation which induced more charge transport. Thus the enhancement of the output voltage of thicker PDMS dielectric layer is much higher than that of thinner PDMS dielectric layer.

The output power for each group by changing the load resistance is shown in Fig. 2(b). The change of the maximum output power for each group follows the same trend as that of open circuit output voltage as shown in Fig. 2(a).

### 3.2. Optimization and evaluation of the liquid flow sensor

In Eq. (1), the spacing between the top surface of the TEH and another contact surface is also another parameter to determine the output voltage. In order to investigate the effect of the spacing between the TEH surface and contact surface, which is the height of the PDMS chamber, we changed the spacing from 250  $\mu\text{m}$  to 1000  $\mu\text{m}$ . In this test, the TEH samples are with pyramid surface micro-pattern and of 215  $\mu\text{m}$  PDMS thickness, which are the samples generating the highest output voltage in Fig. 2(a). The sample was assembled above the top layer of pump-chamber as shown in Fig. 1. The bottom layer of the pump-chamber was pressed to delivery solution of certain volume within the range from 0.01 ml to 0.1 ml. The output voltage was recorded and the relation between the delivery volume and output voltage is shown in Fig. 3(b). According to the Eq. (1) for fully contact-mold TEHs, the output voltage will increase with the increase of the spacing. But as shown in Fig. 3(a), the output voltage decreases with the increase of the spacing. This is because the TEH shown in Fig. 1 is not working in fully contact-mold. With the same deformation of the top layer of the pump-chamber, the contact area decreases with the increase of the spacing. Although the TEH could give higher output voltage when the spacing was lower, the standard deviation was also higher, which is shown as the error-bar in Fig. 3(b). Thus there is a trade-off between the accuracy and the output voltage of the TEH delivery volume sensor. When the pump chamber is pressed by finger, the TEH patch will deform and contact with the Al surface. However, these two surfaces not only contact with each other but also squeeze each other and further have a friction between them. So the whole TEH does not only work in contact mode but also partially works in friction mode.

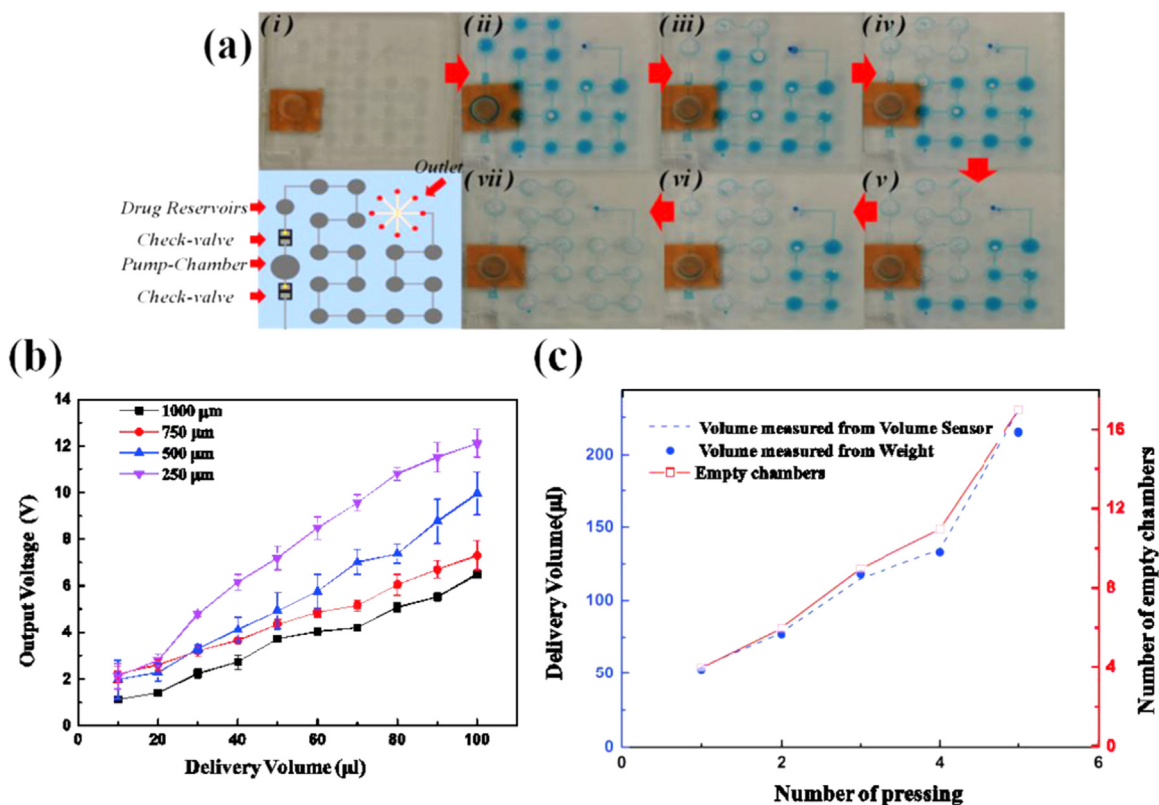


**Fig. 3.** Volume sensor monitors the delivery volume of each pressing of the pump chamber. (a) Demonstration of the drug delivery with volume sensor monitoring; (b) Optimization for spacing between the top and bottom surface of the triboelectric pair; (c) Delivery volume calibration with different measuring method.

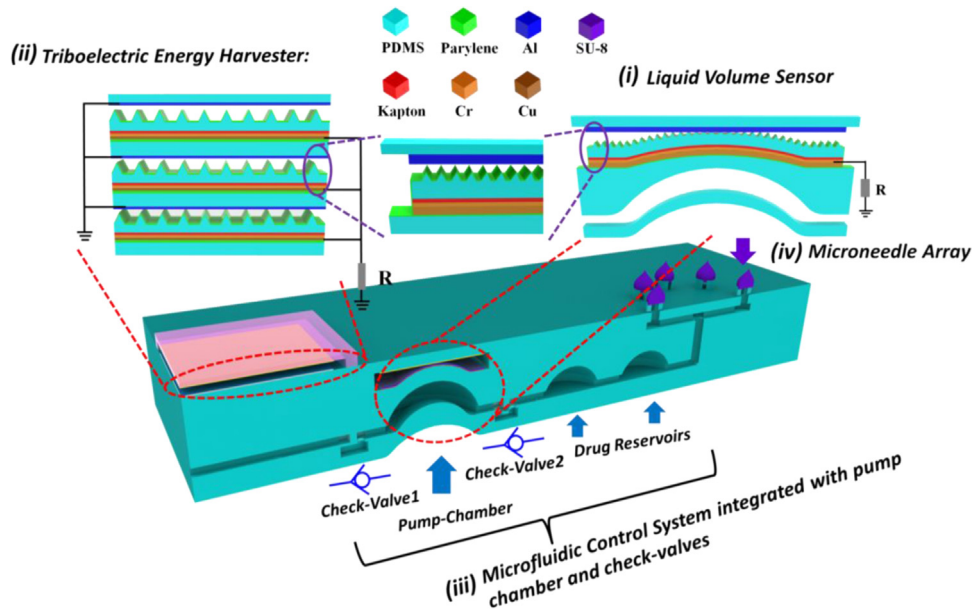


**Fig. 4.** Detailed structure and functional components of lab-on-chip drug delivery patch (i) liquid volume sensor; (ii) triboelectric energy harvester as power supply for active components; (iii) microfluidic control system to fluidic control; (iv) microneedle array to skin penetration before drug delivery.

The friction will also contribute to the output voltage. This friction is more obvious when the spacing is lower. This is because with the same force applied on the pump chamber, the TEH patch will squeeze the Al surface more when the spacing is lower. If the force applied onto the pump chamber is not perpendicular to the Al surface, then a friction will occur. However, the direction of the force applied by human finger cannot be too well controlled. Thus, the extent of friction also cannot be well controlled. This is the reason why the error bar is larger when the spacing is lower. When the spacing is 1000  $\mu\text{m}$ , this friction almost does not happen because the deformation of the TEH surface is not large enough to squeeze the Al surface. Based on the data when the spacing is 1000  $\mu\text{m}$ , the Coefficient of Variation is  $\%CV = 11\%$ . To have a better accuracy for the delivery volume monitoring, the design of 1000  $\mu\text{m}$  spacing was applied for the sample in other tests.

A demonstration of the drug delivery with volume sensor monitoring is shown in Fig. 4(a). The weight of the patch was measured after each pressing to calculate the volume of the delivered solution. And the output voltages of the delivery volume sensor were also recorded and converted to delivered volume according to the voltage–volume curve calibrated in Fig. 3(b). Moreover, the number of empty drug reservoirs can be counted to roughly estimate the delivered drug volume. The results of the delivery volume of each finger-pressing measured by these three methods are shown in Fig. 3(c). The number of empty drug reservoirs for each pressing is 4, 2, 3, 2 and 6, which is indicated as red line in Fig. 3(c). The volume measured by the weight and delivery volume sensor is indicated as blue spots and dash line, respectively. The delivered volume measured by delivery volume sensor and weight is almost the same except to the last data point, i.e., the volume measured by delivery volume sensor is a bit higher than the volume measured by weight. The applied force recorded by the delivery volume sensor at the last finger-pressing data point was higher than the required force to deliver the rest solution in the patch, where the accurate volume is characterized as weight. Secondly the delivered volume measured by counting the empty chamber does not perfectly match with the data measured by delivery volume sensor and weight because there was some residual solution in the empty drug reservoirs and channels. Generally the delivered volume can be roughly and straightforwardly estimated by counting the number of empty drug reservoirs. Thus

the triboelectric volume sensor is required to figure out relatively precise delivered volume as long as some usage scenarios need the information of accurate delivered volume.

### 3.3. Development of the lab-on-chip drug delivery system

We further integrated two functional components within the lab-on-chip drug delivery patch as shown in Fig. 4. A microneedle array was assembled at the position for outlets for skin penetration thus the device can be used for transdermal drug delivery.

On the top surface of the patch, we further integrated a TEH of  $2 \times 2 \text{ cm}^2$  area, which leverages the similar structure of the liquid volume sensor for a further integration of active components. By pressing the TEH from the top, energy can be generated. The detailed fabrication process of the whole device with all functional components is shown in Fig. S3.

### 3.4. Characterization and optimization for the TEH of stacked layers design

Due to the small area of the whole device, the power generated by a single layer of TEH is limited. Thus TEHs of stacked layer design [33–36] have been applied to enhance the output voltage. Multi-TEHs ( $N$  layers) are stacked layer by layer and connected in parallel to achieve a  $N$ -times charge transferred by one pressing comparing with the single layer TEH. If all the  $N$ -layered TEH has the charge transport simultaneously, the total transferred charge will increase  $N$  times. Meanwhile, due to the parallel connection of all layers in the  $N$ -layered TEH, the total inner resistance will decrease, which further enhances the output power.

Here we study the TEH with one, two and three stacked layers. The contact surface of the TEH is parylene vs Al. The thickness of PDMS dielectric layer is 215  $\mu\text{m}$  which is optimized for the highest output (Fig. 2(a)). And to avoid a collapse and contact between two triboelectric surfaces when pressing is not applied, the spacing between two triboelectric surfaces is 700  $\mu\text{m}$ .

In order to calculate the power generated by the TEH, a load resistor was connected between the top and bottom electrodes. A cyclic force of approximately 6 N with 0.5 Hz frequency was applied to generate the power. The voltage was then measured across the load resistor to obtain the power generated by the TEH.

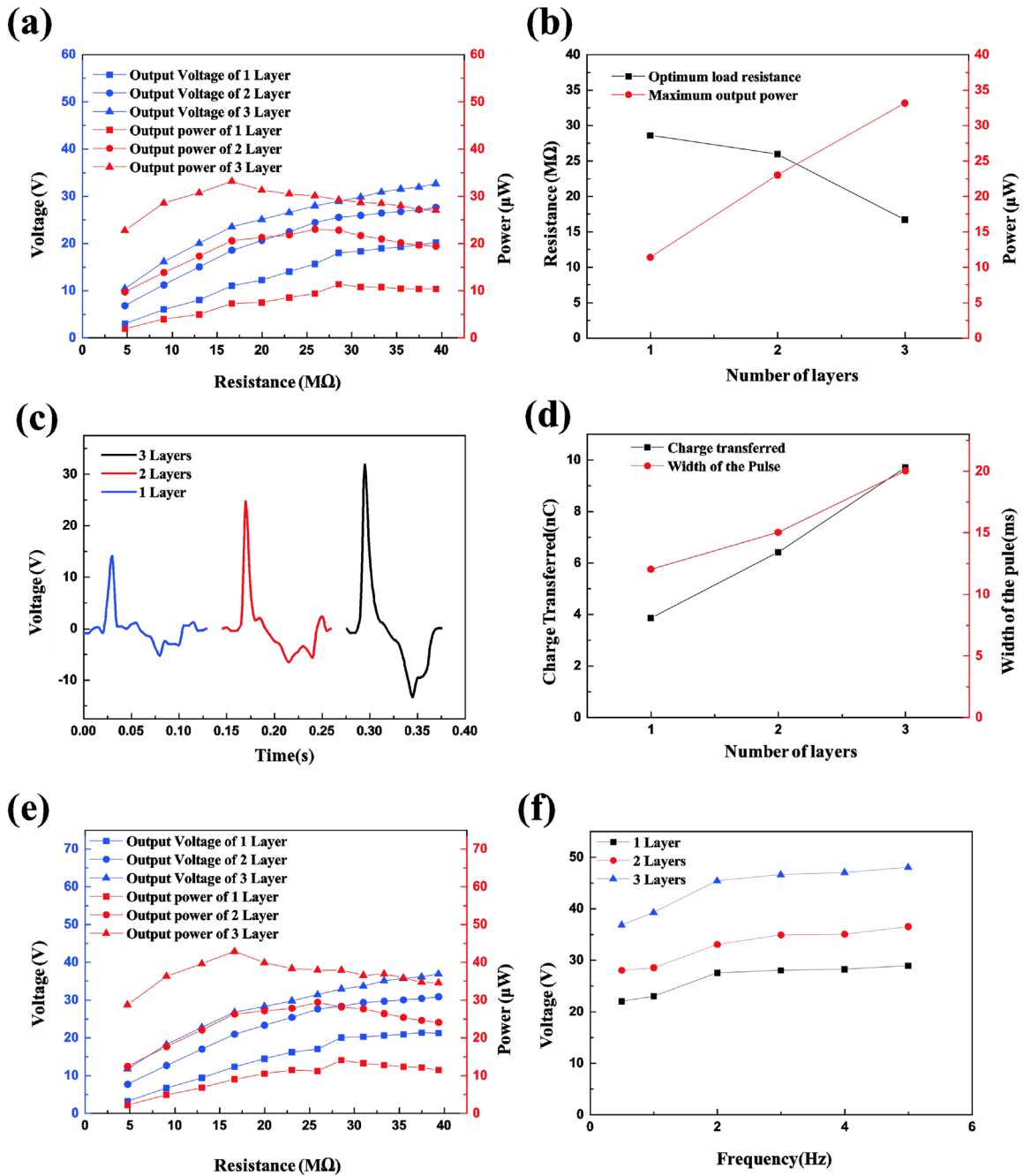


Fig. 5. Characterization and optimization for the TEH of stacked layers design.

As the load resistance was increased, the power output increased and peaked at a point and started dropping thereafter. The voltage and power characteristics of TEH with different stack layers are shown in Fig. 5(a). The maximum power output for devices with one, two and three stacked layers are 11.34 μW, 22.96 μW and 33.12 μW, respectively; the load resistance are approximately 28.57 MΩ, 25.93 MΩ and 16.67 MΩ, respectively, as shown in Fig. 5(b). This decrease of load resistance for peak power represents the decrease of the inner impedance of stacked TEHs, which is induced by the parallel connection of stacked TEHs. The quantity of charge transferred is proportional to the number of layers (black line in Fig. 5(d)), the peak voltage with respect to the number of layers does not follow the same trend. The peak voltage of TEH with 3 layers for open circuit is 33 V while the peak voltage (15 V) of TEH with 1 layer in open circuit is 15 V (Fig. 5(c)). Since all

the triboelectric surfaces cannot be triggered simultaneously for the TEH with more than 1 layer, the voltage pulses of different layers will be generated at different times. Thus the width of voltage pulse will increase with the number of stacked layers (red line in Fig. 5(c)). The finger-pressing frequency will also change the output voltage as shown in Fig. 5(f). As shown in this figure, the peak voltage has an obvious increase within the range from 0.5 Hz to 2 Hz and tends to saturate when frequency is higher than 2 Hz. One major parameter which seems to affect the output voltage was the impact force provided by the finger tip. During manual cyclic pressing test, the amplitude of acceleration or force increases when the cyclic pressing frequency increases. Higher impact force results in increased elastic deformation in the PDMS layer which leads to increased contact area between the two triboelectric layers. The increased contact area is possibly the reason

for increased triboelectric generation and performance of the device (Fig. 5(f)). The output voltage over time generated by different pressing frequency is added in the supplementary information. A representative example of the time domain signals of open circuit output voltage from different frequency with 1 stacked layer is shown in Fig. S7. Considering that the TEH is manually pressed, 2 Hz should be a reasonable optimum operation frequency.

Due to the reliability concern (referring to Fig. S3), a parylene coating on the bottom PDMS dielectric layer was used to protect the metal layer at the backside in our design as shown in the Fig. S3. An experiment has been conducted for the TEHs without parylene coating as a comparison to previous data with parylene in order to characterize the impact of such parylene coating. Thus, the contact surface is PDMS vs Al. The voltage and power characteristics of TEH with different stack layers are shown in Fig. 5(e). Compared with the results of TEH with parylene coating, the load resistances of peak powers are the same. However, the peak powers are  $14 \mu\text{W}$ ,  $29.3 \mu\text{W}$  and  $42.8 \mu\text{W}$ , respectively, indicating an average of 27% enhancement. This result suggests that, if the backside metal of the TEH patch is not easily detached or scratched, the parylene layer can be avoided and PDMS surface can offer a better performance.

### 3.5. Characterization of the liquid volume sensor in insulin delivery test

In order to confirm that the device has ideal features for an efficient drug volume control, transdermal delivery of insulin was tested *in vivo*. As a powerful approach for various biomedical researches such as transdermal drug delivery [39] and transdermal bio-sensing [40], a microneedle array was assembled onto the skin patch for the skin penetration and insulin delivery. The sharp tips

of microneedles were assembled by double drawing lithography [37,38] onto the patch as shown in Fig. 6(a) and (b). A detailed illustration of the double drawing lithography can be found in Fig. S4. Penetration tests on mouse cadaver skin were conducted to characterize the penetration capability of the SU-8 microneedles made by double drawing lithography. A histology image of the skin at the site of one microneedle penetration confirms that the sharp conical tip was not broken during the insertion steps as shown in Fig. 6(c). A detailed *in vitro* drug delivery test is shown in Fig. S6.

All the procedures were performed under protocol and approved by the Institutional Animal Care and Use Committee at the National University of Singapore. Sprague–Dawley rats with weight of 200–250 g were injected with  $50 \text{ mg kg}^{-1}$  streptozotocine (Sigma-Aldrich, Singapore) in citrate buffer (pH 4.2) *via* intraperitoneal injection to generate a diabetic animal model. These rats were kept with free access to food and water for 3 days. Then their blood glucose level was checked by a glucometer (Accu-Chek, USA). The rats with blood glucose level between 16 and 30 mM were selected and the hairs on the abdomen skin were removed by a razor 24 h before the experiment. All these rats were divided into 3 groups and each group contained 3 rats.

We first conducted the tests without liquid volume control to confirm the drug delivery capability of the patch. Group 1 was a negative control group, in which we only tested the blood glucose level throughout the duration of the test. Group 2 was an experimental group. After the rats were anesthetized, the patch with insulin loaded was applied on the abdomen skin surface. The pump chamber was pressed to deliver all the insulin ( $10 \text{ IU mL}^{-1}$ ) contained in the drug reservoirs. As mentioned before, the totally volume of all the drug reservoirs is about  $246 \mu\text{L}$ . In group 3, after the rats were anesthetized,  $10 \text{ IU mL}^{-1}$  Lispro insulin was injected

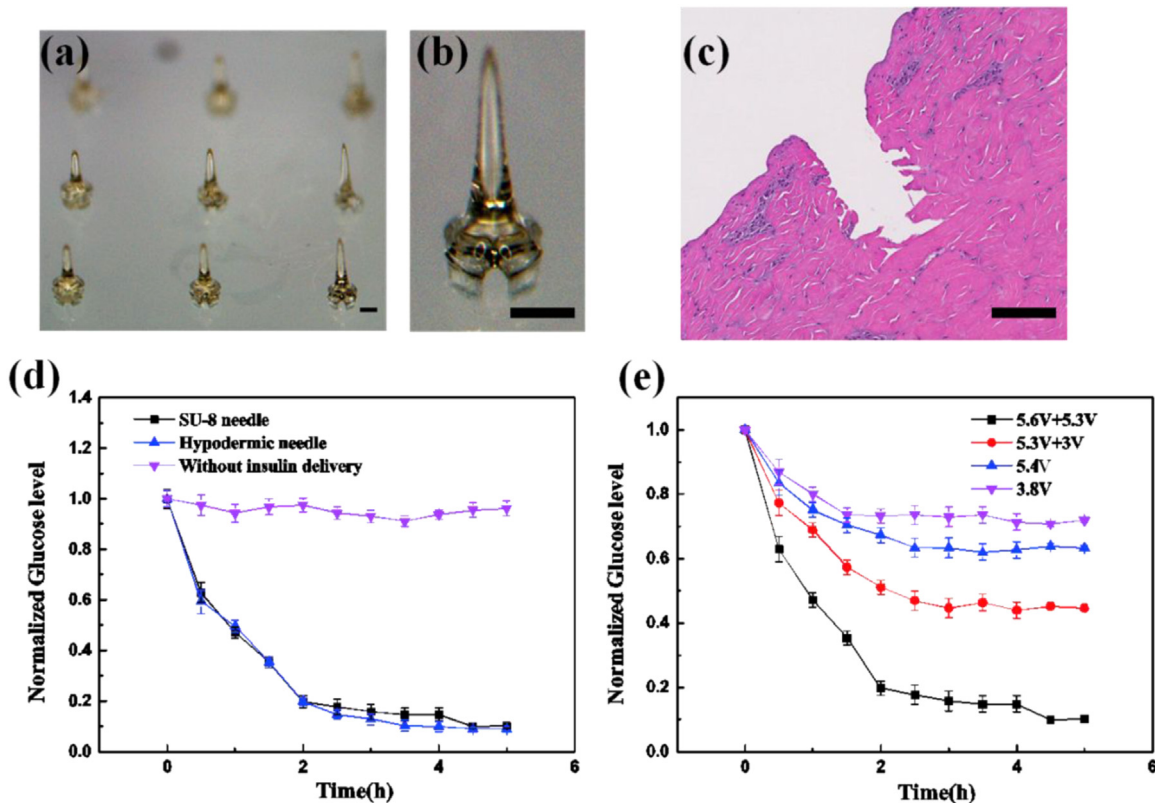


**Fig. 6.** Delivery volume sensor monitors and controls the dose for insulin delivery. (a) Optical image of the microneedle array assembled onto the patch, the scale bar is  $200 \mu\text{m}$ ; (b) Detailed optical image of an individual microneedle, the scale bar is  $200 \mu\text{m}$ ; (c) Histology image of individual microneedle penetration, scale bar is  $200 \mu\text{m}$ ; (d) Changes in blood glucose level in diabetic rats after insulin delivery using microneedles, subcutaneous hypodermic injection of insulin, and without injection of insulin; (e) Changes in blood glucose level in diabetic rats after insulin delivery using microneedles with different delivery volumes.

subcutaneously with a 29G hypodermic needle into the rats (2.5 IUkg<sup>-1</sup>) as a positive control experiment.

Blood samples were taken from the tail vein every 30 min after the beginning of the experiments in all groups. The blood glucose level monitoring lasted for 5.5 h. A glucometer (Accu-Chek, USA) was used to give the corresponding blood glucose levels. The results are shown in Fig. 6(d). The blood glucose level in rats treated with our patch dropped continuously during the 5.5 h insulin delivery period and was quite stable after 3 h. It was significantly different compared with the negative control group, where insulin solution was not administered to the rats. Remarkably, the changing of the blood glucose level in the positive control experiments in both groups, i.e., using patch and a hypodermic needle, was about the same. This experiment successfully proved the feasibility of using proposed LoC drug delivery patch to deliver macromolecules like insulin.

A detailed study was conducted in order to study the ability of manual control function for insulin delivery, which is supported by the microfluidic control system including pump chamber, check-valves and liquid volume sensor. During the test with patches, the delivery volume was controlled by controlling the pressing force. The output voltage of the liquid volume sensor was recorded to confirm the different volume delivered during the tests, as shown in Fig. 6(e). There were 4 groups in the study. For the first 2 groups, only one time pressing was applied during the test. The output voltages of the delivery volume sensor were 3.8 V and 5.4 V, respectively. For the last 2 groups, the pump chambers were pressed twice and the output voltages of the delivery volume sensor were measured as 5.3 V + 3 V and 5.6 V + 5.3 V, respectively. The change of the blood glucose level is shown in Fig. 6(e). For the group with higher voltage output, which means a larger volume of insulin delivery, the blood glucose level drops more. But for all the groups, the blood glucose level stabilized at a certain level after 3 h. The experiment confirms that the manual control delivery mechanism with liquid volume sensor can successfully monitor insulin delivery and further control the blood glucose level. However, during the insulin delivery, the microneedles were immersed within the skin, making the outlets of the microneedles. Thus, the flow resistance of the whole microfluidic channel has a significant increase, result in a slight deviation of the actual delivery volume from the *in vitro* calibration as shown in Fig. S5. Generally speaking, the actual delivery volume of *in vivo* was around 10% lower than that of *in vitro* calibration in the situation of drug delivery when microneedles were in skin.

#### 4. Conclusion

Triboelectric energy harvester has been applied for various kinds of wearable sensors and electronics due to its flexible and thin film structure. Here a liquid volume sensor which leverages the triboelectric mechanism was integrated within a wearable lab-on-chip drug delivery patch to realize a manually controlled large volume drug delivery function. To power active components which will be integrated on the patch in the near future, a stacked layer triboelectric energy harvester (TEH) design was studied and characterized. Increasing the number of stacked layers significantly enhances the output power. The output power generated by a TEH with 3 stacked layers and a 2 × 2 cm<sup>2</sup> area is 33 μW. The optimum pressing frequency is 2 Hz which is within the reasonable range of usage scenarios based manually finger pressing. The liquid volume sensor integrated within the patch leverages the similar structure as the TEH. The spacing between triboelectric pair surfaces is optimized to be 1000 μm for a best accuracy. Thus, the delivery volume can be monitored, which is crucial for certain medical applications such as insulin delivery,

whose delivery dose needs to be precisely controlled. Microneedle array was assembled onto the patch to confirm the drug delivery and volume monitoring functions by *in vivo* experiments in rats. The liquid volume sensor can be integrated with other drug delivery devices or lab-on-chip microfluidic devices when the liquid volume delivered should be accurately measured.

#### Appendix A. Supplementary material

Supplementary data associated with this article can be found in the online version at <http://dx.doi.org/10.1016/j.nanoen.2016.02.054>.

#### References

- [1] L. Atzori, A. Iera, G. Morabito, The internet of things: A survey, *Comput. Netw.* 54 (15) (2010) 2787–2805.
- [2] A.J. Jara, M.A. Zamora, A.F. Skarmeta, An internet of things–based personal device for diabetes therapy management in ambient assisted living (AAL), *Personal. Ubiquitous Comput.* 15 (4) (2011) 431–440.
- [3] C.D. Chin, V. Linder, S.K. Sia, Lab-on-a-chip devices for global health: Past studies and future opportunities, *Lab. Chip* 7 (1) (2007) 41–57.
- [4] X. Huang, Y. Liu, H. Cheng, W.-J. Shin, J.A. Fan, Z. Liu, C.-J. Lu, G.-W. Kong, K. Chen, D. Patnaik, S.-H. Lee, S. Hage-Ali, Y. Huang, J.A. Rogers, Materials and designs for wireless epidermal sensors of hydration and strain, *Adv. Funct. Mater.* 24 (2014) 3846–3854, <http://dx.doi.org/10.1002/adfm.201303886>.
- [5] Suh, Kahp-Yang, Noo Li Jeon, and Changhyun Pang, “Wearable skin sensor using programmable interlocking of nanofibers.” *Nano/Micro Engineered and Molecular Systems (NEMS)*, 2013 8th IEEE International Conference on IEEE, 2013.
- [6] L.M. Strambini, A. Longo, S. Scarano, T. Prescimone, I. Palchetti, M. Minunni, D. Giannessi, G. Barillaro, Self-powered microneedle-based biosensors for pain-free high-accuracy measurement of glycaemia in interstitial fluid, *Biosens. Bioelectron.* 66 (2015) 162–168.
- [7] Y. Yoon, G.S. Lee, K. Yoo, J.B. Lee, Fabrication of a microneedle/CNT hierarchical micro/nano surface electrochemical sensor and its *in-vitro* glucose sensing characterization, *Sensors* 13 (12) (2013) 16672–16681.
- [8] Joshua Windmiller, Nandi Ray, Min-Chieh Zhou, Gabriela Chuang, Padmanabhan Valdés-Ramírez, Philip R. Santhosh, Roger Miller, Narayan, Joseph Wang, Microneedle array-based carbon paste amperometric sensors and biosensors, *Analyst* 136 (9) (2011) 1846–1851.
- [9] Philip R. Miller, Shelby A. Skoog Thayne, L. Edwards, Deanna M. Lopez, David R. Wheeler, Dulce C. Arango, Xiaoyin Xiao, Susan M. Brozik, Joseph Wang, Ronen Polsky, Roger J. Narayan, Multiplexed microneedle-based biosensor array for characterization of metabolic acidosis, *Talanta* 88 (2012) 739–742.
- [10] Samjin Choi, Zhongwei Jiang, A novel wearable sensor device with conductive fabric and PVDF film for monitoring cardiorespiratory signals, *Sensors Actuators A: Phys.* 128 (2) (2006) 317–326.
- [11] O. Veisheh, R. Langer, Diabetes: A smart insulin patch, *Nature* 524 (7563) (2015) 39–40.
- [12] I.C. Lee, J.S. He, M.T. Tsai, K.C. Lin, Fabrication of a novel partially dissolving polymer microneedle patch for transdermal drug delivery, *J. Mater. Chem. B* 3 (2) (2015) 276–285.
- [13] Yaowu Bai, Timothy Miller, Mingjuan Tan, Lawrence Siu-Chun Law, Tong Joo Gan., Lidocaine patch for acute pain management: a meta-analysis of prospective controlled trials, *Curr. Med. Res. Opin.* 31 (3) (2015) 575–581.
- [14] Hulin Zhang, Ya Yang, Te-Chien Hou, Yuanjie Su, Chenguo Hu, Zhong Lin Wang., Triboelectric nanogenerator built inside clothes for self-powered glucose biosensors, *Nano Energy* 2 (5) (2013) 1019–1024.
- [15] R. Zhang, S. Wang, M.H. Yeh, C. Pan, L. Lin, R. Yu, Z.L. Wang, A streaming potential/current-based microfluidic direct current generator for self-powered nanosystems, *Adv. Mater.* (2015).
- [16] Lin Zong-Hong, Guang Zhu, Yu. Sheng Zhou, Ya Yang, Peng Bai, Jun Chen, Zhong Lin Wang, A self-powered triboelectric nanosensor for mercury ion detection, *Angew. Chem. Int. Ed.* 52 (19) (2013) 5065–5069.
- [17] Zong-Hong Lin, Gang Cheng, Wenzhuo Wu, Ken C. Pradel, Zhong Lin Wang, Dual-mode triboelectric nanogenerator for harvesting water energy and as a self-powered ethanol nanosensor, *ACS Nano* 8 (6) (2014) 6440–6448.
- [18] Zhong Lin Wang, Triboelectric nanogenerators as new energy technology for self-powered systems and as active mechanical and chemical sensors, *ACS Nano* 7 (11) (2013) 9533–9557.
- [19] Caofeng Pan, Zetang Li, Wenxi Guo, Jing Zhu, Zhong Lin Wang, Fiber-based hybrid nanogenerators for/as self-powered systems in biological liquid, *Angew. Chem.* 123 (47) (2011) 11388–11392.
- [20] Long Lin, Yannan Xie, Sihong Wang, Wenzhuo Wu, Simiao Niu, Xiaonan Wen, Zhong Lin Wang., Triboelectric active sensor array for self-powered static and dynamic pressure detection and tactile imaging, *ACS Nano* 7 (9) (2013) 8266–8274.

- [21] Feng-Ru Fan, Long Lin, Guang Zhu, Wenzhuo Wu, Rui Zhang, Zhong Lin Wang., Transparent triboelectric nanogenerators and self-powered pressure sensors based on micropatterned plastic films, *Nano Lett.* 12 (6) (2012) 3109–3114.
- [22] Yufang Li, Gang Cheng, Zong-Hong Lin, Jin Yang, Long Lin, Zhong Lin Wang., Single-electrode-based rotary triboelectric nanogenerator and its applications as self-powered contact area and eccentric angle sensors, *Nano Energy* 11 (2015) 323–332.
- [23] Chang Han, Chi Bao, Xiao Hui Zhang, Limin Li, Tao Zhang, Weiguo Zhou, Hu, Zhong Lin Wang, Self-powered velocity and trajectory tracking sensor array made of planar triboelectric nanogenerator pixels, *Nano Energy* 9 (2014) 325–333.
- [24] Mengdi Han, Xuming Xiao-Sheng Zhang, Bo. Meng Sun, Wen Liu, Haixia Zhang, Magnetic-assisted triboelectric nanogenerators as self-powered visualized omnidirectional tilt sensing system, *Sci. Rep.* 4 (2014).
- [25] Jun Chen, Guang Zhu, Weiqing Yang, Qingshen Jing, Peng Bai, Ya Yang, Te-Chien Hou, Zhong Lin Wang, Harmonic-resonator-based triboelectric nanogenerator as a sustainable power source and a self-powered active vibration sensor, *Adv. Mater.* 25 (42) (2013) 6094–6099.
- [26] Ya Yang, Hulin Zhang, Jun Chen, Qingshen Jing, Yu. Sheng Zhou, Xiaonan Wen, Zhong Lin Wang, Single-electrode-based sliding triboelectric nanogenerator for self-powered displacement vector sensor system, *ACS Nano* 7 (8) (2013) 7342–7351.
- [27] Yuanjie Su, Guang Zhu, Weiqing Yang, Jin Yang, Jun Chen, Qingshen Jing, Zhiming Wu, Yadong Jiang, Zhong Lin Wang, Triboelectric sensor for self-powered tracking of object motion inside tubing, *ACS Nano* 8 (4) (2014) 3843–3850.
- [28] Ya Yang, Guang Zhu, Hulin Zhang, Jun Chen, Xiandai Zhong, Zong-Hong Lin, Yuanjie Su, Peng Bai, Xiaonan Wen, Zhong Lin Wang, Triboelectric nanogenerator for harvesting wind energy and as self-powered wind vector sensor system, *ACS Nano* 7 (10) (2013) 9461–9468.
- [29] Bo Meng, Wei Tang, Zhi-han Too, Xiaosheng Zhang, Mengdi Han, Wen Liu, Haixia Zhang, A transparent single-friction-surface triboelectric generator and self-powered touch sensor, *Energy Environ. Sci.* 6 (11) (2013) 3235–3240.
- [30] Guang Zhu, Wei Qing Yang, Tiejun Zhang, Qingshen Jing, Jun Chen, Yu. Sheng Zhou, Peng Bai, Zhong Lin Wang, Self-powered, ultrasensitive, flexible tactile sensors based on contact electrification, *Nano Lett.* 14 (6) (2014) 3208–3213.
- [31] Ya Yang, Hulin Zhang, Zong-Hong Lin, Yu. Sheng Zhou, Qingshen Jing, Yuanjie Su, Jin Yang, Jun Chen, Chenguo Hu, Zhong Lin Wang, Human skin based triboelectric nanogenerators for harvesting biomechanical energy and as self-powered active tactile sensor system, *ACS Nano* 7 (10) (2013) 9213–9222.
- [32] S. Niu, S. Wang, L. Lin, Y. Liu, Y.S. Zhou, Y. Hu, Z.L. Wang, Theoretical study of contact-mold triboelectric nanogenerators as an effective power source, *Energy Environ. Sci.* 6 (12) (2013) 3576–3583.
- [33] M. Kanik, M.G. Say, B. Daglar, A.F. Yavuz, M.H. Dolas, M.M. El-Ashry, M. Bayindir, A motion- and sound-activated, 3d-printed, chalcogenide-based triboelectric nanogenerator, *Adv. Mater.* 27 (14) (2015) 2367–2376.
- [34] Yeong Ko, Goli Hwan, Nagaraju, Jae Su Yu, Multi-stacked PDMS-based triboelectric generators with conductive textile for efficient energy harvesting, *RSC Adv.* 5 (9) (2015) 6437–6442.
- [35] Cheng Gang, Li Zheng, Zong-Hong Lin, Jin Yang, Zuliang Du, Zhong Lin Wang, Multilayered-electrode-based triboelectric nanogenerators with managed output voltage and multifold enhanced charge transport, *Adv. Energy Mater.* (2014).
- [36] Po-Kang Yang, Zong-Hong Lin, Ken C. Pradel, Long Lin, Xiuhua Li, Xiaonan Wen, Jr-Hau He, Zhong Lin Wang, Paper-based origami triboelectric nanogenerators and self-powered pressure sensors, *ACS Nano* (2015).
- [37] Z. Xiang, H. Wang, A. Pant, G. Pastorin, C. Lee, *Biomicrofluidics* 7 (2013) 26502.
- [38] Z. Xiang, H. Wang, A. Pant, G. Pastorin, C. Lee, *Biomicrofluidics* 7 (2013) 66501.
- [39] Y.-C. Kim, J.-H. Park, M.R. Prausnitz, Microneedles for drug and vaccine delivery, *Adv. Drug. Deliv. Rev.* 64 (2012) 1547.
- [40] L. Ventrelli, L.M. Strambini, G. Barillaro, Microneedles for transdermal bio-sensing: current picture and future direction, *Adv. Healthc. Mater.* (2015), <http://dx.doi.org/10.1002/adhm.201500450>.